08,16

Metal-organic halide perovskites structured by detonation-synthesis nanodiamonds. Elements of the model and the ways for experimental verification

© N.I. Alekseyev[1,2], A.N. Aleshin[1], G.V. Nenashev[1], I.V. Oreshko[1,2], N.N. Zhogal[2], Z. Hongkai[2]

[1] Ioffe Institute,
St. Petersburg, Russia
[2] St. Petersburg State Electrotechnical University „LETI"
St. Petersburg, Russia

E-mail: NIAlekseyev@yandex.ru

Received November 14, 2025
Revised November 14, 2025
Accepted November 16, 2025

This paper is devoted to interpretation of the research of a hybrid metalorganic perovskite film of the methylammonium-Pb-halogen$_3$ type modified with detonation-synthesized nanodiamonds. The most striking of these results is the ability of the film to partially restore their differential conductivity G after a significant initial decrease during the periods of several to tens of days. The interpretation is based on modeling the rather complex structure of fields generated by functional groups at the periphery of the nanodiamond particles, which reach values on the order of interatomic fields.

Keywords: halide perovskites, nanodiamonds, detonation synthesis, differential conductivity, quantum chemical modeling.

DOI: 10.61011/PSS.2025.12.63085.324-25

1. Introduction

We have established a number of unusual properties of films of organometallic hybrid perovskites (HP) in Ref. [1] which were observed during their modification by detonation nanodiamonds (DND) particles. The most significant is the ability of the films to partially restore their differential conductivity G, which has been decreasing since the beginning of the experiments (as with all HP [1]) after a considerable time, i.e. several dozens of days. It should be noted that the initial decrease in conductivity of G during the first few days was not too large (no more than 50 %).

This paper is devoted to the interpretation of the observed trends, as well as to the discussion of the voltage characteristics of modified hybrid perovskite. We would like to recall that HP perovskites are a class of materials with the general formula $ABX3$, where A is an organic functional group, for example, methylammonium (MA) or formamidium (FA), B is a heavy metal atom (the most common variant is lead Pb), X is a heavy halogen (usually iodine or bromine); the latter component is associated with the second variant of the abbreviation HP — halide perovskite [2].

Hybrid perovskites are characterized by high light-absorbing properties, charge transfer ability, and simplicity of chemical solution methods in synthesis and processing. Over time, the potential of HP was realized in other applications such as memristive structures [3], light-emitting diodes and lasers [4], photodetectors, ferroelectrics. The latter application looks natural if we recall classical ferroelectrics with a perovskite lattice structure — barium titanates, lead, strontium, potassium niobate and a number of others [5]. Ferroelectric properties are currently found in both classic HP [6] and new ones developed specifically to improve the basic parameters of ferroelectrics — polarizability and Curie temperature [7].

Ferroelectric HP are mentioned here in connection with a possible interpretation of the remission of differential conductivity in the final part of Ref. [1]. The interpretation appeals to the occurrence of built-in electric fields in the volume of HP. Indeed, almost the entire volume occupied by perovskite grains is located in the area of fields created by subsurface layers of nanodiamonds and functional groups (FG) on their surface. If the volume fraction of nanodiamonds is approximately equal to their mass concentration $\eta = 0.01$, then the average distance D between DND particles (conventionally packed into a cubic lattice) is $D \approx r_{ND}(4/\eta)^{1/3}$. At $r_{ND} = 5$ nm, it is equal to 40−50 nm, i.e. it is only an order of magnitude larger than the radius DND (this can be seen from Figure 2, *b* in Ref. [1]). Since the film composite then analyzed is formed from a solution by crystallization of HP grains around DND, D can be associated with the size of a cluster forming around a DND particle. For brevity, we will continue to call it an HP cluster (in fact, each such cluster is a polycrystal of a large number of HP single crystals).

The interface electric field F at the boundary of the functional group layer (FG) with HP is further evaluated in sign and magnitude. It is inferior to the characteristic values of interatomic fields (having the order of units of V/Å) by no more than an order of magnitude, i.e. it is tenths of V/Å, and can be either positive or negative.

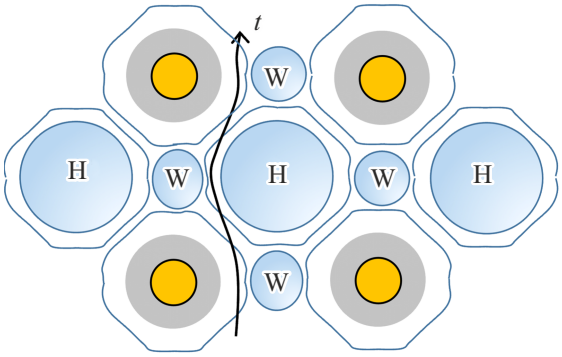

Figure 1. Perovskite structuring scheme around diamond nanoparticles (DND — yellow) and surrounding layers of functional groups (gray). The entire volume outside the functional groups is the volume of perovskite. H and W are areas of hillocks and wells. Arrow is the migration trajectory of halogen ions along an electric field applied in the same direction. Gray lines are potential isolines.

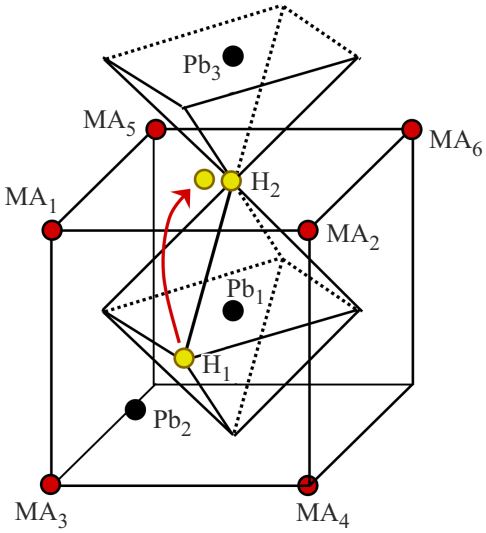

Figure 2. An HP lattice cell structured around an octahedron of H_1-H_2 anion halides (highlighted in yellow), in case of the transition of H_1 to a position near H_2.

HP clusters of dielectric perovskite around DND particles have no electric charge. Therefore, the potential structure within clusters and taking into account the field F at the interfaces with DND has the form of potential hillocks H and wells W (Figure 1). The wells in Figure 1 are located along the shortest distance between the nearest neighbors, the tops of the hillocks are located along the main diagonals of the cubic cells.

The arrangement of H and W in Figure 1 refers to the case of a well for halogen anions along the axis connecting the nearest diamond nanoparticles. In this case, the interface electric field pushes the anions away from the outer boundary of FG. When the field sign is opposite, the hillocks H and the wells W change places on this boundary. However, in any case, when an external electric field is applied, the trajectory of the halogen anion traverses the slopes of hillocks and wells, as shown by the black arrow t (trajectory), bypassing wells and hillocks. In this case, the area of halogen drift trajectories in the form of a narrow band around the line t is depleted of halogens escaping as a result of electromigration.

As in conventional, unmodified HP, these halogen anions can escape further through the cathode and leave the film area, impairing its characteristics. In HP, modified DND, replenishment of outgoing halogen anions in current channels t during current flow and during pause periods occurs due to diffusion from wells W (against the electric field) and from hillocks down (along the field).

The times of these two diffusions are sharply different with a field value of F close to the interatomic fields. In the general case, the diffusion rate is determined by the activation barrier E_a of the exit of the halogen anion from its position in the perovskite lattice. In various sources [8,9] E_a, calculated by quantum chemistry methods (semi-empirical or DFT), gives 0.2−0.6 eV. Knowledge of E_a allows estimating the probability of the transition of the halogen anion to an adjacent position in the HP lattice (Figure 2), the diffusion coefficient and mobility in a weak external field, based on the basic formulas of chemical kinetics [10]. However, in a strong field of the field scale F, the barrier E_a changes by an amount of the order of the E_a itself in the direction of decreasing (in case of diffusion from a hillock) or increasing (in case of diffusion from a well). If we take $E_a = 0.5$ eV, then the diffusion rate proportional to $\exp(-E_a/T)$ changes by 9 orders of magnitude in one direction or the other. With a mobility of μ of the order of 1 cm^2/Vs (in a weak field), the effective diffusion coefficient D_{diff} from the well (against the field F) is no more than $3 \cdot 10^{-11}$ cm^2/s, turning wells into a long-term storage tank for halogens and providing partial restoration of the perovskite structure over long time intervals.

The time to exit the tank has the order of r_w^2/D_{diff} (where r_w is the radius of the wells W), strongly depends on E_a and can even be hours and days. On the other hand, during the current flow, the halogen-depleted flow channel is replenished by rapid (almost instantaneous) diffusion from the hillocks. The uncertainty of the value E_a smoothens out the difference in the sizes of the regions H and W between the case shown in Figure 1 and the opposite (when H and W are reversed). It is significant, however, that a fairly regular pattern of wells and hillocks, contributing to the retention and creation of a reservoir of halogen anions, exists only under conditions of n- or p- doping of DND particles. The impurities in this case are nickel and the traditional diamond dopants — boron and phosphorus [11].

2. Modeling of doped DND particles with different functional groups on their surface

As already mentioned, the field strength F at the outer boundary of the layer of functional groups of DND particles

inside the HP cluster is determined by the polarity of the groups and the field at the interface of the doped (or undoped) DND particle. The upper boundary of F is the order of the ratio of the energy of the Coulomb interaction of charges of the nearest atoms, to which a localized charge is attributed ξe, to the interatomic distance r_{12} (e — elementary charge, $\xi < 1$). If we are not talking about strongly electronegative atoms (oxygen), then $\xi \sim 0.1$. Then the energy of interaction of charges in eV is equal to the ratio $\xi_1\xi_2/(r_{12}/r_0)$, where $r_0 = 14.4\,\text{Å} = 1.44 \cdot 10^{-7}$ cm is the distance between charges „e", at which the Coulomb energy is 1 eV. For $r_{12} = 1.4\,\text{Å}$ $\xi_1\xi_2/(r_{12}/r_0) \sim 0.1$ eV, $F \sim 10^7$ V/cm. In relation to perovskite, the field F plays the role of an external one.

If we compare F with the saturating field HP as a ferroelectric, then with the polarizability expressed in μC(microculon)/cm^2 (that is, in units of the surface charge density of the capacitor, the charge Q/(area A)), the effective field is $4\pi Q/(\varepsilon A)$ in the CGS or $Q/(\varepsilon\varepsilon_0 A)$ system in SI. For $Q/A = 1$, this field is equal to $1.1 \cdot 10^7/\varepsilon$ V/cm, which corresponds to the value calculated above. For $MaPbI_3$, the permeability ε is approximately equal to 50 [6], and the susceptibility of $Q/A \sim 0.3$ (for a number of more modern HP, the Q/A value is much higher, several units [7]). Therefore, the internal fields at the boundaries of the functional groups correspond to the limiting polarization of perovskite as a ferroelectric.

On the other hand, the external fields in the middle part of the HP film are much smaller when the film is operating in the memristive cell mode: $F_{\text{mean}} \sim 6 \cdot 10^4$ V/cm. Indeed, if we estimate the mobility of halogen ions and halogen vacancies at the level of $\mu_{\text{Hal,vac}} \sim (1-10)\,\text{cm}^2/\text{Vs}$, and the density of ion-vacancy plasma is $10^{18}\,\text{cm}^{-3}$, then the current density calculated for the Fmean field is many orders of magnitude higher than the observed one [9]. This means that almost all the voltage applied to the film is localized in the electrode layers. As for the built-in field F, it is significantly larger than F_{mean}, and when analyzing the „DND-groups-HP" system, the latter can be ignored altogether.

When evaluating F_{mean} given above, we encounter a fundamental issue in the physics of HP perovskites, which we have already addressed in Ref. [9]: the enormous mobility of halogen anions and the difficulty of fixing the state of the film as a memristive system under voltage relief. In fact, the mobility of anions in the near-electrode layers of perovskite is many orders of magnitude lower and it limits the conductivity of the film. We will return to this problem when discussing the volt-ampere characteristics of HP films in Sec. 4.

The simplest way to model the potential profile in an HP cluster is to construct a potential curve through a chain of volumes occupied by individual atoms. The chain should include the axial elements of the functional group on the surface of the DND particle and their natural continuation into the structure of the DND particle (in one direction) and the ball HP shell (in the other). The averaged potential curve can be constructed from the Poisson equation if charges are known that are conditionally localized on the atoms of the chain. The conventionality of this procedure is due to the fact that the distribution of charge in space between the nearest atoms is very difficult.

In this case, the specific type of atoms in the composition of the functional group, in the DND particle and in the perovskite should be „familiar" to this package. From this point of view, no problems arise with diamond doped with its traditional light impurities (boron and phosphorus) and common functional groups (hydroxy, carboxy, amino groups, epoxy bridges). Information about the charge distributions on the atoms of these structures is provided by semi-empirical methods of quantum chemistry, for example, in the most easy-to-use package HyperChem [12], which is optimal at the same time when working with molecular (rather than periodic) objects, which are „DND-particle — perovskite" complexes.

In a number of cases, we also turned to the Quantum Espresso package, which uses density functional theory (DFT) methods, contains data on heavy perovskite atoms (lead, bromine, and caesium), and is convenient when working with periodic lattices. Unfortunately, Espresso does not provide information about the distribution of charges and has difficulty combining objects that are too different in their morphology.

It should be noted that a correct solution to a second-order boundary value problem with two zero conditions for a normal derivative at the edges of the region under study (an HP cluster as an analog of a conditional elementary HP cell) cannot be constructed. Therefore, we limited ourselves to considering the segment from the DND center to the middle of the segment in the direction of the other DND closest to it (with the coordinate $r = D/2$), and set a zero condition on the derivative at this point ($r = D/2$). The reliability of the solution was assessed by the fact that in the depth of the DND particle (where no condition was formally set), the potential curve monotonously flattens out and its derivative is close to zero. At the same time, there were no problems related to the formal incorrectness of the task.

First, we considered the structure of a diamond (the simplest component of a composite to model) with a zero potential derivative inside it and functional groups open to the outside. This is how the fields that appear on the outside of these groups were evaluated.

The problem of the potential change near the interface of variously doped (or completely undoped) diamond is closely related to the actual problems of diamond physics: negative electron affinity (NEA) and acceptor conductivity near a diamond superficially doped with hydrogen, and both of these circumstances are interpreted ambiguously [13,14].

It is generally assumed that the profile of the potential n- of an doped semiconductor near the interface behaves similar to the potential profile inside a metal, which prevents the escape of electrons (Figure 3). For n-diamond (Figure 3, *a*) it weakly depends on whether the interface atom of the semiconductor is in contact with the hydrogen

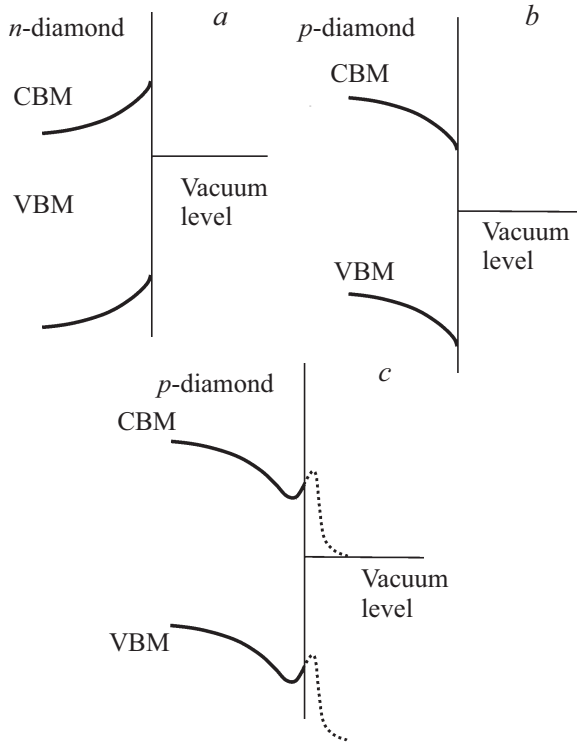

Figure 3. Traditional bending schemes of zones at the interface of doped diamond with vacuum.

atom H or oxygen O of the OH group. The situation with *p*-doped semiconductor is less clear (we will talk specifically about diamond). The simplest profile shown in Figure 3, *b* and facing the curve *a* is modified depending on the functional group. The direction of charge transition from the interface carbon to the adatom is difficult to specify in case of contact with the simplest such group — H-adatom. The NEA variant corresponds to the electron transition from hydrogen to carbon. An additional „nibble" appears on the curve *b* in case of the transition towards hydrogen (Figure 3, *c*), which can manifest itself as an area of acceptor conduction. However, the reason for this conductivity may be the penetration of hydrogen into the crystal as an acceptor impurity.

With such ambiguity, it is convenient to turn to quantum chemical modeling and test various options. Initially, diamond fragments were constructed within the framework of the semi-empirical AM1 method of the HyperChem package, which were not doped in volume, then — doped with boron or phosphorus in various layers (111) parallel to the interface (i. e., in the volume of the fragment). Then external atoms were added: an oxygen atom, either bound to the interface atom C, or connected to it through an intermediate hydrogen atom. The remaining surface of the diamond fragment, not bound to FG, was doped with hydrogen. To minimize the edge effects, we considered an excessively „thick" diamond — in 4 double planes of atoms (111) with a total number of atoms of about 400.

The inset in Figure 4 shows a section of such a diamond fragment perpendicular to the line of sight [111], and curves of change in the average charge density along the line of atoms 0-1-…-5 (bold dots in the inset of Figure 4); the last atom of this chain is −hydrogen.

In the averaging procedure used, the charge ξe localized on the atom was matched to the value on the continuous charge density curve. At nodal points, this value was obtained by dividing the charge by the tabular volume of a given type of atom. Thus, a sixth-order polynomial was constructed for the second derivative and the eighth-order polynomial was constructed for the value of the potential). An alternative is to construct a sequence of Gaussian functions blurred around the local charges of atoms; this approach does not fundamentally change the results.

It can be seen that the potential change curve in Figure 4 is qualitatively quite consistent with the NEA concept. On the contrary, the introduction of *p*-impurity atom (boron) directly at the interface eliminates NEA (Figure 5).

A number of other characteristic inter-positions of the internal doping atom and fragments of external functional groups are shown in Figures 6, 7. The curves *1* in these figures reproduce the second derivative of the potential and the potential itself in Figure 4. Other options are indicated on the curves by the color of the circles. It can be seen that when the doping atom B is moved to „the second row" of double diamond planes (111), the monotonously decreasing potential profile (i. e., a hint of NEA) can be traced along a normal that does not directly pass through the doping atom (Figure 6, curves *2* and *3*). To simplify the construction of curves in Figure 6, it was assumed that the positions of atoms along the line of sight [111] (axis x) on all curves are the same, which, of course, is not entirely true.

The oxygen atom adjacent to the interface carbon atom in the form of an OH fragment always only passivates

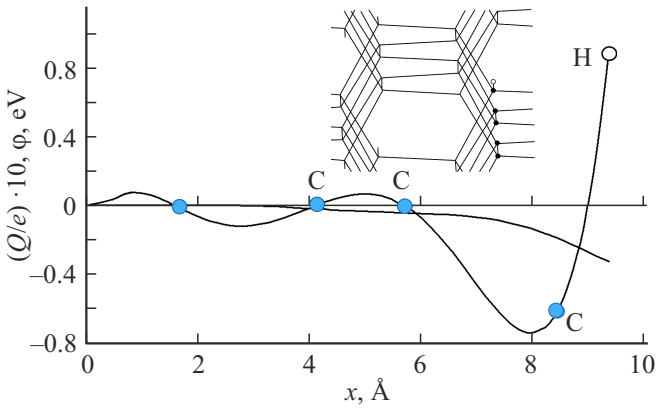

Figure 4. The profile of the second derivative φ'' of the potential and the potential φ at the interface of the (111) diamond plane with a hydrogen adatom on the „protruding" atom C (φ'' is represented through conditional charges localized on individual atoms). φ'' — oscillating curve, potential — monotonic curve. The right-to-left direction on the graph corresponds to the bottom-to-top movement during insertion.

the diamond surface, which is well known from the experiment — curve *4* in Figures 5, 6. The displacement of the oxygen atom to a position external to the diamond nanoparticle or the introduction of a phosphorus donor impurity into the diamond does not change anything (the corresponding curves are not shown).

The presented results are not new, however, they allow us to assess the adequacy of potential construction based on discrete charges given by HyperChem and the procedures for processing these data. For the perovskite problem, the most important of these results is the magnitude of the field at the end of the functional group external to the diamond. In all cases shown in Figures 6, 7, this field is (0.5–2) V/Å.

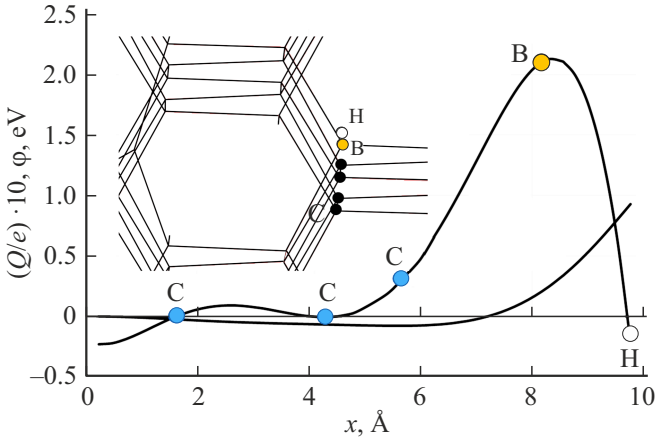

Figure 5. The same as in Figure 4, with one *p*-doping atom (boron highlighted in yellow) directly on the line of sight.

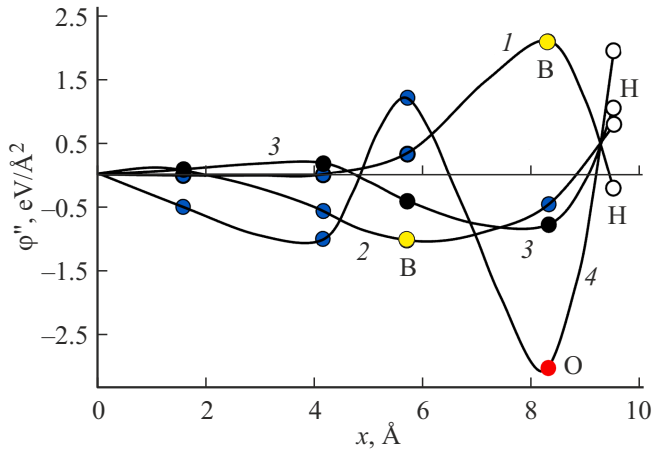

Figure 6. The change in the second derivative of the potential obtained by interpolating charges on diamond atoms (carbon or impurity) and atoms of functional groups produced by HyperChem. The curve *1* reproduces the curve *1* in Figure 3; the boron atom has been moved to the second row of diamond atoms on the curve *2*; *3* — curve through a normal parallel to the normal of the curve *2* and not passing through boron atoms B (yellow): *4* — hydroxyl radical OH on an undoped diamond. O atom is highlighted in red.

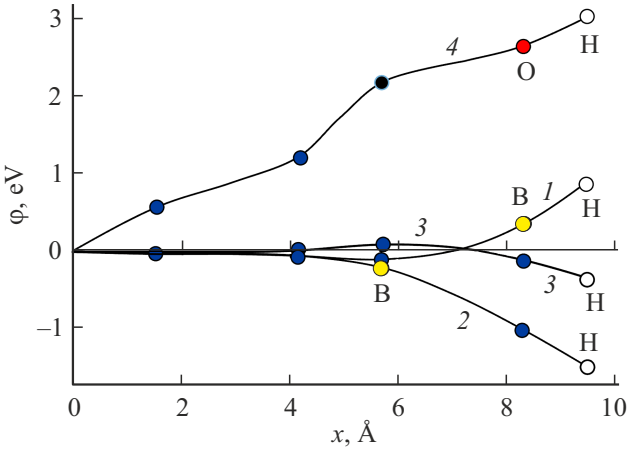

Figure 7. The change in potential corresponding to its second derivative is shown in Figure 4. The explanations on the curves are similar to Figure 5.

The nature of the change in this value is estimated below when the group is loaded on both sides.

3. Modeling of perovskite nanoparticles structured around an doped DND particle through functional groups on its surface

As mentioned above, modeling the nanoparticle ensemble of hybrid perovskite is difficult due to the heavy metal atoms and the bulkiness of the structure of the organic component of HP-perovskite — methylammonium or formamidium. But for the interpretation of the HP results, the most important question is how much the polarization field inside the perovskite is affected by the asymmetry of the „DND particle–functional groups–perovskite“ structure and how much this field changes compared to the case of „free end“ functional group. Therefore, initially believing that the specificity of perovskite for qualitative consideration may be unprincipled, we initially replaced it with an undoped diamond. A characteristic change in the potential profile for this case is shown in Figures 8, 9. In this case, the field between the oxygen atom and the interface atom of the right DND particle is almost identical to that on the outside of the functional group of the OH chain, which is not connected to anything. The same trend is observed when doping a nanodiamond particle with various dopants.

For a composite material including nanodiamond particles and perovskite grains structured around it, the configuration of functional groups is formed around an doped diamond when interacting with electric fields on its surface (resulting from doping). In this case, a functional group (for example, an OH group) turns out to have a positive (or negative) charge both towards and away from the nanoparticle — this depends on the type of doping. For example, the oxygen of the OH group can be combined with the carbon atom of

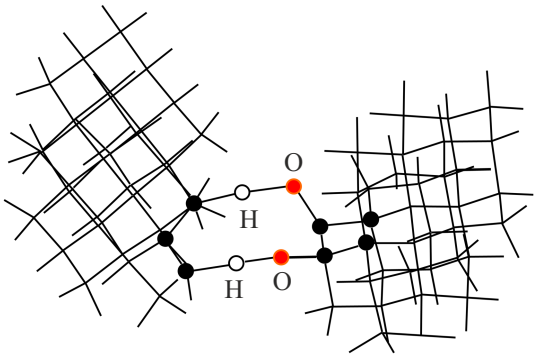

Figure 8. Two undoped nanodiamond particles connected through the OH functional group.

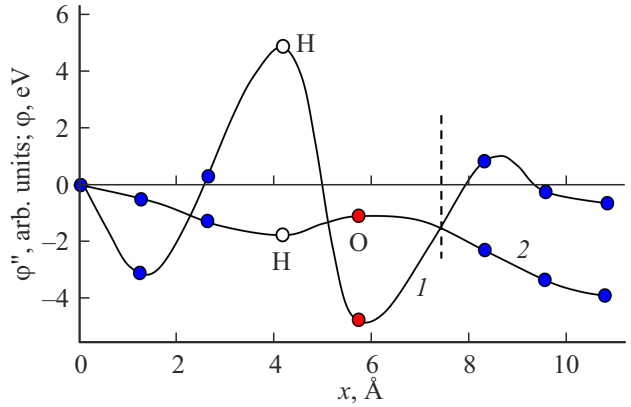

Figure 9. Change of the second derivative of the potential φ'' (curve *1*) and the potential φ (curve *2*) through the functional group and its extensions inside DND particles. Dotted line is a conditional boundary of the right undoped DND particle.

Figure 10. Two undoped DND particles connected to a central, doped DND particle.

the left DND particle and the hydrogen atom belonging to the right particle.

In this case, the formal valence of hydrogen is disrupted and its bond with the right DND is similar to the donor-acceptor bond (hereinafter, for brevity, DA). However, the HyperChem package used „sees“ a similar relationship, even if it is not formally specified. In this case, the position of the oxygen atom can be called internal. On the contrary, at the „external“ position of the oxygen atom for a free DND particle that is not connected to other DNDs, some of the oxygen atoms are interconnected by DA bonds. When the „doped DND group“ complex is introduced with an undoped DND particle, these bonds should partially transfer to the atoms of this DND particle. Thus, optimization of a single doped DND particle and two ND particles connected through groups should be performed separately.

In addition, modeling of the „doped DND particle–group–undoped DND particle“ is more correct if it is performed for a symmetric system that includes two undoped DND particles on either side of the central particle (which itself can be undoped) and functional groups „included“ towards each other — Figure 10.

All the considered options are presented in Table 1. Since the images provided by HyperChem are very faded, and redrawing the structure as a whole is quite laborious, we limited ourselves to conditional schemes. Zero binding energy for each of the two types of $-$CO and NH_2 groups considered — corresponds to the central undoped DND particle and this direction of connecting the groups to the lateral undoped DND particles (rows 1, 7 in the table related to CO and NH_2 groups). The opposite directions of group connection for the same central undoped DND particle give a different configuration binding energy (lines 4 and 10 for CO and NH_2 groups, respectively). This applies both to the unloaded central DND particle (column 1 in all rows, energy $|E_{\text{doped}}^{\text{unloaded}}| - |E_{\text{undoped}}^{\text{unloaded,line1}}|$ for the OH group or $|E_{\text{doped}}^{\text{unloaded}}| - |E_{\text{undoped}}^{\text{unloaded,line7}}|$ for the NH_2-group) and to the loaded — second columns with energy $|E_{\text{doped}}^{\text{loaded}}| - |E_{\text{undoped}}^{\text{loaded,line1}}|$ or $|E_{\text{doped}}^{\text{loaded}}| - |E_{\text{undoped}}^{\text{loaded,line7}}|$. The third and fourth columns indicate the absolute value of the electric field strength $|F_{\text{outer}}|$ either at the outer boundary of the group not loaded with an undoped DND particle ($|F_{\text{outer}}^{\text{unloaded}}|$) or at the boundary with this DND particle ($|F_{\text{outer}}^{\text{loaded}}|$ — dotted line in Figure 10). Rows (2-3), (5-6) for the OH group and similar ones for the NH_2-groups show changes in the binding energy for unloaded — column 1, and loaded groups during doping of the central DND particle — column 2. Columns 3, 4 give the field strengths at the group boundaries.

The overall result of the table can be formulated as follows. The maximum amount of binding energy is provided by the direction of group attachment, in which the combination with the bending of the potential inside the DND particle gives an alternation of positive and negative charges. For example, with *n*-doping (phosphorus), which creates, on average, a concavity of the potential curve inside the right interface of the central doped DND particle down (minus), the maximum of $|E_{\text{bond}}|$ is provided by the conversion of the H atom in the OH group to the DND particle and oxygen – outside. With *p*-doping, the opposite happens. This result can be considered as expected. Less obvious is that in this case, the maximum increment in the magnitude of the electric field is provided at the boundary with the undoped DND particle. On an intuitive level, this is probably due to the fact that two regions of negative charge, „included“ one after the other, are mutually weakened. An undesirable alternation of charge signs gives a result that differs little from the case of an undoped central DND particle. This applies both to the binding energy of the

Table 1. Different configurations of bound DND particles

	$\lvert E_{doped}^{unloaded}\rvert - \lvert E_{undoped}^{unloaded,line1}\rvert$	$\lvert E_{doped}^{unloaded}\rvert - \lvert E_{undoped}^{unloaded,line1}\rvert$	$\lvert F_{outer}^{unloaded}\rvert$	$\lvert F_{outer}^{loaded}\rvert$
(C...−C) ··HO−(C−...−C...−C)−OH···(C−...−C)	0	0	0.46	0.42
(C...−C) ··HO−(C−...−B...−C)−OH···(C−...−C)	−0.4	−0.56	0.63	0.35
(C...−C) ··**HO**−(C−...−**P**...−C)−**OH**···(C−...−C)	−1.2	−1.42	1.28	1.23
(C...−C)−OH···(C−...−C...−C)···HO−(C−...−C)	0.7	1.05	0.35	0.57
(C...−C)−OH···(C−...−**B**...−C)···HO−(C−...−C)	−1.45	−2.15	1.13	1.36
(C...−C)−OH···(C−...−P...−C)···HO−(C−...−C)	0.90	1.25	0.24	0.79
	$\lvert E_{doped}^{unloaded}\rvert - \lvert E_{undoped}^{unloaded,line7}\rvert$	$\lvert E_{doped}^{unloaded}\rvert - \lvert E_{undoped}^{unloaded,line7}\rvert$	$\lvert F_{outer}^{unloaded}\rvert$	$\lvert F_{outer}^{loaded}\rvert$
(C−C) ··HNH_2−(C−..C...−C)−NH_2H···(C−...−C)	0	0	0.36	0.4
(C−C) ··HNH_2−(C−..B...−C)−NH_2H···(C−...−C)	−0.33	−0.26	0.53	0.45
(C−C) ··HNH_2−(C−..P...−C)−NH_2H···(C−...−C)	−1.44	−1.32	1.62	1.43
(C−C)−NH_2H···(C−...−C...−C)···HNH_2−(C−C)	0.56	1.25	0.15	0.5
(C−C)−NH_2H···(C−...−B...−C)···HNH_2−(C−C)	−1.45	−2.05	1.32	1.16
(C−C)−NH_2H···(C−...−P...−C)···HNH_2−(C−C)	0.83	1.37	0.24	0.59

Table 2. Variants of configurations of bound DND particles taking into account the influence of hybrid perovskite

	$\lvert E_{doped}^{unloaded}\rvert - \lvert E_{undoped}^{unloaded,line1}\rvert$	$\lvert E_{doped}^{unloaded}\rvert - \lvert E_{undoped}^{unloaded,line1}\rvert$	$\lvert F_{outer}^{unloaded}\rvert$	$\lvert F_{outer}^{loaded}\rvert$
(C...−C) ··HO−(C−...−C...−C)−OH···HP	0	0	0.36	0.40
(C...−C) ··HO−(C−...−B...−C)−OH···HP	−0.66	−0.79	0.60	0.31
(C...−C)−OH···(C−...−C...−C)···HO−HP	0.93	1.25	0.54	0.59
(C...−C)−OH···(C−...−B...−C)···HO−HP	−1.25	−1.59	1.10	1.06

system and to the magnitude of the electric field in the external undoped DND particle — a perovskite simulator.

In the absence of doping of DND particles, the central particle contacts both different poles of functional groups and groups of different types. In this case, the sign of the electric field at the boundary of the external functional group turns out to be undefined, and its magnitude is minimal.

To understand the specifics of perovskite in terms of fields induced by functional groups, a minimal lattice fragment was constructed that allows these groups to be attached to the centers of the perovskite interface (100). Enstatite $MgSiO_3$, a material known in geology, was chosen as a model perovskite. Perovskite is not the only variant of the crystal lattice for $MgSiO_3$, but the parameters of the perovskite variant are known: $a = 4.780$ Å, $c = 6.902$ Å. HyperChem tools then allow manually entering the coordinates of an acceptable number of atoms point-by-point and use them as a first approximation.

The studied cubic fragment of the $MgSiO_3$ perovskite lattice included eight (23) lattice cells, i.e. 27 magnesium atoms, eight silicon atoms, and 36 oxygen atoms in eight octants. The atoms at the interfaces of the fragment were „counted“ per atom. Thus, 71 atoms were taken into account. Since all perovskite atoms are characterized by high metallicity of bonds, we resorted to the „Arbitrary valence“ option, which allows stitching a fragment with at least a minimal set of bonds — inside halogen octahedra and between magnesium atoms forming a cubic cell around each octahedron. It is noteworthy that the silicon atoms trapped inside the octahedra found their position on their own. The ideal cell layout and the result of optimization using the semiempirical PM3 method are shown in Figure 11, *a*, on the left.

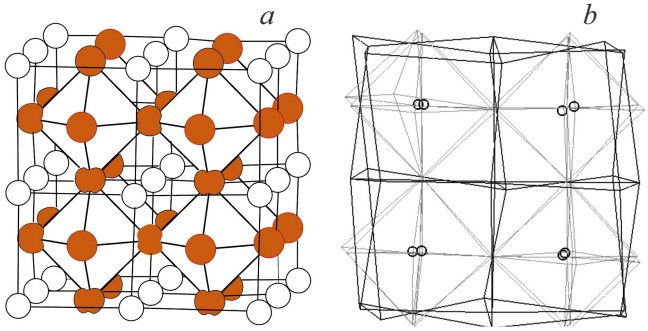

Figure 11. An ideal fragment of the lattice of enstatite $MgSiO_3$, drawn point-by-point (on the left) and the result of optimization of its geometry by the PM3 method in the HyperChem package.

The distortion of the ideal lattice in Figure 10, *b* is very small and allows attaching both a functional group and a nanodiamond particle to the HP molecule. In most cases, the structure could be optimized using the PM3 method.

Below are the data in Table 2, similar to Table 1, in those geometries that allowed us to obtain the result.

It can be seen that it was possible to trace the amplification of the built-in field with the correct alternation of charge signs only in one case (row 4), which is close to row 5 of the previous table. The effect of this field on the migration of halogen ions and positive vacancies occurring in HP was evaluated in section 2.

4. Volt-ampere characteristics of HP films structured with nanodiamonds

The waxes of composite material films described in Ref. [1] are basically similar to the volt-ampere characteristics obtained without the introduction of a nanodiamond structurator. Their analysis requires a detailed consideration of stationary current transfer in HP films, taking into account such HP specifics as the ease of release of Hal^- halogen ions from the lattice (i.e., the smallness of their activation energy) and the formation of a pair „vacancy–halogen anion“ („Vac^+–Hal^-“). The concentration of pairs in this case is many orders of magnitude higher than the concentration of „ordinary“ semiconductor carriers — electrons and holes, reaching values of the order of $10^{18}\,cm^{-3}$ [8,9]. A separate article will be devoted to a detailed description of the current passage in HP, which develops our earlier studies [10]. Here we will limit ourselves to a brief summary of the results obtained.

The existence of migration and anion-vacancy (hereinafter for short — a-v-) conductivity strongly affects the band structure of HP as a semiconductor. In Figure 12, the gold electrode (conventionally — cathode) in contact with the HP film forms contact with another metal with a slightly higher output. With short-circuited electrodes and in the absence of migration, the CBM level inside doped semiconductors should lead to the formation of two Schottky barriers with a potential well between them (Figure 12, *b*). However, this requires free electrons or holes, i.e., doped HP (the concentration of native carriers in HP as a fairly wide-band semiconductor is small). It can be assumed that the migration of the halogen ion along the diagonal of the halogen octahedron (Figure 2), leading to the formation of „vacancy-halogen ion pairs“ („Vac^+–Hal^-“) [8,9], also leads to the appearance of just such „ordinary“ carriers — electrons and holes. The system of zones of these carriers, which partially fall into the HP band gap, depends on the concentration of „Vac^+–Hal^-“ pairs, i.e. on temperature.

At the same time, in the presence of migration and a large number of pairs, a potential change curve is formed (the bold curve in Figure 12, *c*), similar to the potential profile in some types of gas discharge (for example, high-pressure thermionic discharge). However, at low voltage on the HP

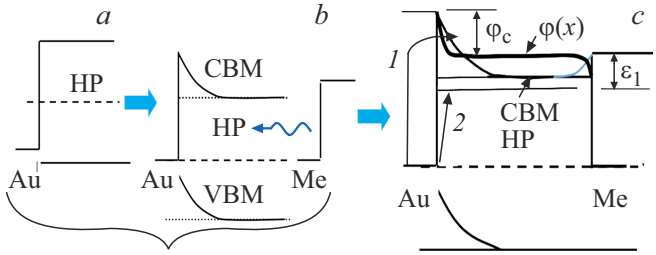

Figure 12. A scheme for the formation of an equilibrium level of CBM when electrodes come into contact with halide perovskite HP. *a* — the left electrode (cathode) of Au with HP when they conditionally approach; *b* — the cumulative structure of HP-Au-Me with the right electrode (Me — metal); *c* — CBM levels and potential profile $\varphi(x)$ formed by anion halides and vacancies.

film, this curve has almost no relation to current transfer, since the Fermi level of the metal cathode is much lower than the potential profile and the metal electrons cannot recombine with positive vacancies suitable to the left edge of the film. Indeed, at the difference in Fermi levels between the metal and perovskite $\Delta\varepsilon = 5.1-3.36 = 1.74\,eV$ (figures are taken from [15,16] and correspond to halide perovskite $MAPbI_3$) and room temperature RT, thermal emission from the metal through the barrier $\Delta\varepsilon$ negligibly small. It is also easy to evaluate direct tunneling through a narrow almost transparent cathode barrier (arrow 1, Figure 12, *c*) in combination with a preliminary thermal energy set of the electron. If the voltage across the film is U, it is divided equally between the cathode φ_c and the anode φ_a (in Figure 12 $U = 0$), each of them is $\varphi_c = \varphi_a = (U/2 + (A_c - A_a)/2)$, where A_c, A_a is the output of the cathode and anode, respectively. Then the tunneling current to the SBM level is estimated from above at $1.1 \cdot 10^7 \cdot \exp(-(\Delta\varepsilon - U/2)/T)$ (if the output operation difference is ignored) and can be at least $1\,nA/cm^2$ only at a sufficiently high voltage on the film $U = 1.6\,eV$. At this voltage alone, the a-v current can manifest itself, no matter how potentially large it is at a given temperature. In this case, the potential profile is almost completely in equilibrium.

At a higher voltage, electrons begin to pass through the cathode barrier, gradually activating the a-v current. The transition to this mode and the change of the dominant current transfer mechanism manifests itself in the form of a fracture of the volt-ampere characteristic, but should not be accompanied by a jump, since with an increase in voltage on the film, the cathode barrier (with a voltage drop φ_c in Figure 12, *c*) expands and the length of the tunneling is increasing.

Another mechanism limiting the growth of the a-v current as the dominant current in the film is a sharp decrease in the mobility of ions and vacancies in the near-electrode layers. The mechanism of this limitation is that the concentration of vacancies (i.e., missing halogen ions) in the cathode layer increases in the direction from the film to the left electrode (cathode) so fast that vacancies can no longer occur.

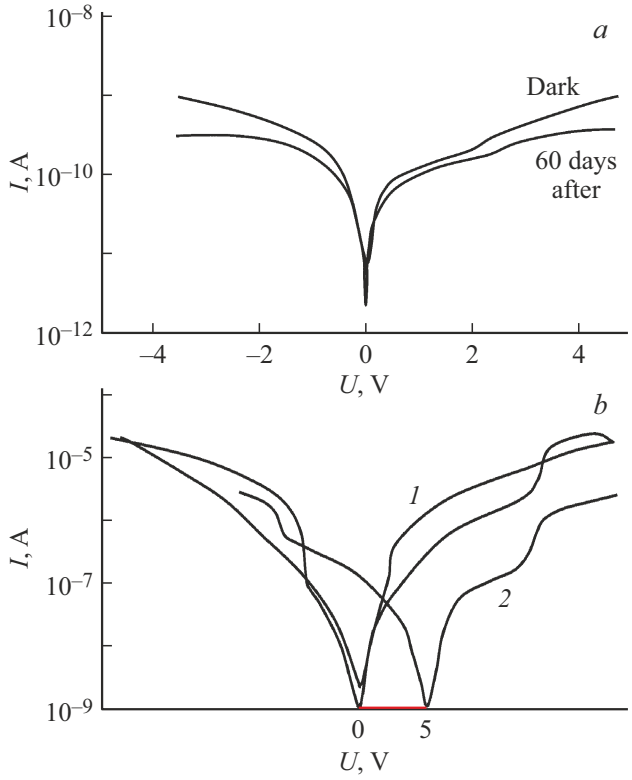

Figure 13. Volt-ampere characteristics of HP structured around *p*-doped nanodiamonds (boron) (*a*) and around the HP-graphene composite (*b*) at different temperatures: curve *1* on (*b*) — at RT, curve *2* — at 220 °s.

From this point of view, it is interesting to analyze the volt-ampere characteristic of the HP film structured with graphene nanoparticles [17,18] at various temperatures. On the curves in Figure 13, *a* corresponding to RT, a weakly pronounced resistive switching is observed, and it is precisely at the voltage on the film $U \sim 2$ V, starting from which electrons from the metal cathode can begin to tunnel into the film body. At a temperature lower than 80 K (Figure 13, *b*, curve *2*), this switching is much less pronounced. This may mean that the a-v current cannot now be considered as indefinitely large, i. e. its activation energy of halogens and vacancies is much higher T.

The second resistive switching is observed at a voltage of about 10 V (in Figure 13, *b*), in our opinion, has nothing to do with the a-v current and may indicate either the beginning of convective splitting of the movement of halogens and vacancies into cells such as Benard cells or the occurrence of delays.

It should be noted that the polycrystalline nature of the HP structure changes almost nothing in the above arguments, as will be shown in a more detailed review.

Conclusion

A hybrid perovskite film modified with detonation synthesis nanodiamonds was modeled to improve the stability of perovskite. The purpose was to explain a number of experimental features in comparison with unmodified film.

In search of a mechanism for restoring the differential conductivity of a hybrid film, we analyzed the structure of the electric fields of clusters forming around nanodiamonds. The migration routes of anion-halogens in the potential relief of clusters revealed the presence of a hierarchy of characteristic times — small depletion times of anion-halogen pathways and replenishment times of these pathways, and the latter turn out to be very large, turning wells into a long-term storage tank for halogens and providing partial restoration of the perovskite structure over long time intervals. It is significant that a fairly regular pattern of wells and hillocks, providing well-separated time decay and recovery of conductivity, is clearly expressed only under conditions of *n*- or *p*-doping of DND particles with traditional diamond dopants such as boron and phosphorus. In this case, modeling that takes into account the interaction of dopant fields inside nanodiamonds and characteristic functional groups on the periphery of nanodiamonds indicates the greatest increase in the binding energy precisely with a certain type of doping.

Further, an interpretation of a small current surge in the form of a resistive switching on the VAC of a modified perovskite at a voltage of about 1.5−2 V is proposed. The jump is associated with the transition from electron current transfer over allowed states inside the perovskite band gap to electron tunneling from the cathode through a narrow cathode barrier created by a dense plasma of halogen ions and positive vacancies at the cathode interface

Conflict of interest

The authors declare that they have no conflict of interest.

References

[1] G.V. Nenashev, A.N. Aleshin, N.I. Alekseev, M.S. Dunaevskiy, V.Yu. Dolmatov. J. Mater. Sci.: Mater. Electron. **36**, 1498 (2025).
[2] D.N. Jeong, J.M. Yang, N.G. Park. Nanotechnology **31**, *15*, 152001 (2020).
[3] S. Liu, J. Zeng, Q. Chen, G. Liu. Front. Phys. **19**, *2*, 23501 (2024).
[4] P. Wang, X. Bai, C. Sun, X. Zhang, T. Zhang, Y. Zhang. Appl. Phys. Lett. **109**, *6*, 063106 (2016).
[5] G.A. Smolensky. UFN **62**, *1*, 41(1957) (in Russian).
[6] S. Yoon, Y. Kim, T. Dang, H.J. Choi, B. Park, J. Eom, H. Song, D. Seol, Y. Kim, S. Shin, J. Nah. J. Mater. Chem. A **4**, *3*, 756 (2016).
[7] R.S. Muddam, L.K. Jagadamma. J. Mater. Chem. C **13**, *21*, 10488 (2025).
[8] A. Walsh, D.O. Scanlon, S. Chen, X.G. Gong, Su-H. Wei. Angew. Chem. **54**, *6*, 1791 (2015).
[9] T. Leijtens, S.D. Stranks, G.E. Eperon, R. Lindblad, E.M. Johansson, I.J. McPherson, H. Rensmo, J.M. Ball, M.M. Lee, H.J. Snaith. ACS Nano **8**, *7*, 7147 (2014).
[10] N.I. Alekseev, A.N. Alyoshin. FTT **66**, *3*, 377 (2024) (in Russian).

[11] N.I. Alekseev, V.V. Luchinin. Elektronika almaza. Izd-vo SPbGETU „LETI“, Sankt-Peterburg (2019). p. 144 (in Russian).
[12] HyperChem. Computational Chemistry, Hypercube Inc. Publication HC50-00-03-00 (1996).
[13] I.L. Kraisky, V.M. Asnin. Appl. Phys. Lett. **72**, *20*, 2574 (1998).
[14] D. Takeuchi, M. Riedel, J. Ristein, L. Ley. Phys. Rev. B **68**, *4*, 041304 (2003).
[15] M. Nasiruddin, M. Vasilopoulou. Global'naya energiya **29**, *1*, 21 (2023) (in Russian).
[16] E.I. Battalova, S.S. Kharintsev. Optika i spektroskopiya **131**, *11*, 1495 (2023) (in Russian).
[17] D.V. Amasev. Fotoelektricheskie yavleniya v tonkih plenkah gibridnyh metallorganicheskih perovskitov na osnove $CH_3NH_3PbI_{33}$. Diss. k.f.-m.n. Moskva, (2023) (in Russian).
[18] G.V. Nenashev, A.N. Aleshin, I.P. Shcherbakov, V.N. Petrov. Solid State Commun. **348**, 114768 (2022).

Translated by A.Akhtyamov